Coherent Dynamics in Quantum Emitters under Dichromatic Excitation

Z. X. Koong[,1,*] E. Scerri[,1,‡] M. Rambach[,1,§] M. Cygorek[,1] M. Brotons-Gisbert[,1]
R. Picard[,1] Y. Ma[,2] S. I. Park[,3] J. D. Song[,3] E. M. Gauger[,1] and B. D. Gerardot[1,†]

[1]SUPA, Institute of Photonics and Quantum Sciences, Heriot-Watt University, Edinburgh EH14 4AS, United Kingdom
[2]College of Optoelectronic Engineering, Chongqing University of Posts and Telecommunications, Chongqing 400065, China
[3]Center for Opto-Electronic Materials and Devices Research, Korea Institute of Science and Technology,
Seoul 02792, Republic of Korea

We characterize the coherent dynamics of a two-level quantum emitter driven by a pair of symmetrically detuned phase-locked pulses. The promise of dichromatic excitation is to spectrally isolate the excitation laser from the quantum emission, enabling background-free photon extraction from the emitter. While excitation is not possible without spectral overlap between the exciting pulse and the quantum emitter transition for ideal two-level systems due to cancellation of the accumulated pulse area, we find that any additional interactions that interfere with cancellation of the accumulated pulse area may lead to a finite stationary population inversion. Our spectroscopic results of a solid-state two-level system show that, while coupling to lattice vibrations helps to improve the inversion efficiency up to 50% under symmetric driving, coherent population control and a larger amount of inversion are possible using asymmetric dichromatic excitation, which we achieve by adjusting the ratio of the intensities between the red- and blue-detuned pulses. Our measured results, supported by simulations using a real-time path-integral method, offer a new perspective toward realizing efficient, background-free photon generation and extraction.

Solid-state quantum emitters, in particular, semiconductor quantum dots (QDs), offer a promising platform for generating quantum states that can facilitate dephasing-free information transfer between nodes within an optical quantum network [1–4]. On-demand indistinguishable photon streams for this purpose can be made using coherent excitation of QDs [5]. While resonance fluorescence of QDs suppresses detrimental environmental charge noise [6] and timing jitter [7] in the photon emission, the excitation laser must be filtered from the single-photon stream. Typically, this is achieved with polarization filtering of the resonant laser. However, unless employing a special microcavity design [8–10], polarization filtering inherently reduces collection efficiency by at least 50%. This motivates the consideration of alternative off-resonant excitation techniques to allow spectral filtering [11]. In particular, off-resonant phonon-assisted excitation [12,13], resonant two-photon excitation [14], and resonant Raman excitation [15] schemes benefit from being able to spectrally isolate the zero-phonon line from the laser spectrum, to enable efficient single-photon generation.

However, the benefits of these nonresonant schemes are accompanied by their intrinsic drawbacks (e.g., emission time jitter [16,17], nuclear spin noise [15,18,19], and excitation-induced dephasing [20,21]), which inevitably degrade the photon indistinguishability. To address these issues, He et al. [22] propose a coherent driving scheme using a pair of pulses, each with envelope $\epsilon(t)$ and detuned by $\pm\Delta$ from the fundamental transition of the emitter ω_0. The idea behind such dichromatic excitation is that the combined effect $f(t)$ of two identical, equally detuned pulses with envelopes $\epsilon(t)$ becomes equivalent to a single resonant pulse with modified envelope $\epsilon'(t) = 2\epsilon(t)\cos(\Delta t)$,

$$
\begin{aligned}
f(t) &= \epsilon(t)\cos[(\omega_0 - \Delta)t)] + \epsilon(t)\cos[(\omega_0 + \Delta)t] \\
&= 2\epsilon(t)\cos(\Delta t)\cos(\omega_0 t) = \epsilon'(t)\cos(\omega_0 t). \quad (1)
\end{aligned}
$$

The argument is that this would make it possible to efficiently excite quantum emitters using pulses that are spectrally separated from the fundamental transition.

However, a different picture unfolds when the system dynamics is considered in more detail: the Hamiltonian of an ideal two-level system (2LS) driven by a dichromatic pulse $f(t) = \epsilon_R(t)e^{-i\Delta t} + \epsilon_B(t)e^{i\Delta t}$ with real envelopes of the red- and blue-detuned pulses $\epsilon_R(t)$ and $\epsilon_B(t)$ (using the rotating wave approximation in the rotating frame with respect to the 2LS) is given by

$$H = \frac{\hbar}{2}[f(t)^*|e\rangle\langle g| + f(t)|g\rangle\langle e|] = \mathbf{\Omega}(t) \cdot \mathbf{s}, \quad (2)$$

$$\mathbf{\Omega}(t) = \begin{pmatrix} \mathrm{Re}\{f(t)\} \\ \mathrm{Im}\{f(t)\} \\ 0 \end{pmatrix} = \begin{pmatrix} [\epsilon_R(t) + \epsilon_B(t)]\cos(\Delta t) \\ -[\epsilon_R(t) - \epsilon_B(t)]\sin(\Delta t) \\ 0 \end{pmatrix}, \quad (3)$$

where we have expressed the two-level state as a pseudo-spin Bloch vector $\mathbf{s}$ precessing about the time-dependent precession axis $\mathbf{\Omega}(t)$.

For identical envelopes $\epsilon_R(t) = \epsilon_B(t) =: \epsilon(t)$ as in Eq. (1), the y component of the precession axis vanishes and the excited state population can be determined analytically as

$$n(t) = \frac{1}{2}\left[1 - \cos\left(\int_{-\infty}^{t} dt' 2\epsilon(t')\cos(\Delta t')\right)\right]. \quad (4)$$

In the limit $t \to \infty$ the integral in Eq. (4) becomes the Fourier transform $\mathcal{F}[f](\omega = 0)$ of $f(t)$, evaluated at the two-level transition frequency. This proves analytically that—irrespective of the driving strength, no excited state population exists after the pulse unless there is overlap between the dichromatic excitation spectrum and the fundamental transition of the quantum emitter.

To illustrate this, Fig. 1(a) presents the dynamics of an ideal 2LS under dichromatic excitation with Gaussian pulses. This shows transient excited state population that, however, vanishes again toward the end of the pulse, i.e., the overall accumulated pulse area does indeed cancel almost completely. The small but finite residual occupation can be explained by the nonzero overlap between the tails of the Gaussians and the fundamental transition. Consequently, coherent Rabi-like oscillations with unity
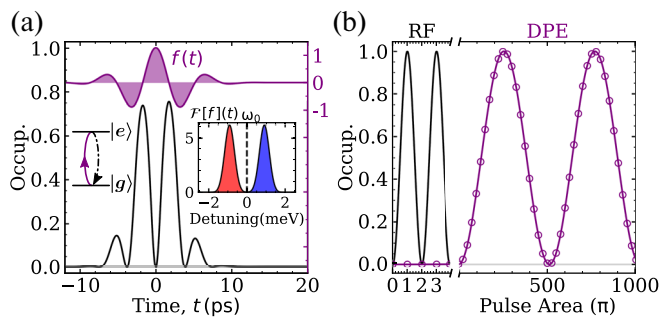

FIG. 1. Symmetric dichromatic excitation of a two-level system. (a) Temporal evolution of the symmetric dichromatic excitation field $f(t)$ (purple) and the associated spectrum [inset, $\mathcal{F}[f](t)$]. The corresponding excited state population (black) upon interaction with the dissipation-free 2LS highlights the vanishing population inversion as a result of the net cancellation of the temporal pulse area. (b) The excited state population as a function of pulse area of the driving field for both monochromatic resonant driving (RF) and DPE. Results from numerical simulation (purple circles) match well with our analytical expression (solid line).

population inversion can still be obtained, albeit at much larger intensities, as depicted in Fig. 1(b). However, this obviously defeats the purpose of employing the dichromatic excitation scheme.

The observation of transient excited state population suggests that significant population inversion can still be obtained even if the exciting pulse has no spectral overlap with the transition of the emitter: Any additional interaction or dissipation can interfere with the complete cancellation of the pulse area and thus lead to a finite population inversion after the pulse. For example, in a laser-driven QD, the interaction with phonons induces incoherent thermalization dynamics in the instantaneous laser-dressed state basis, unlocking population up to $\sim$50%.

In this Letter, we propose and experimentally demonstrate an alternative, externally controllable approach to dichromatic pulsed excitation (DPE). To obtain large stationary occupations of the excited state, we employ asymmetric dichromatic excitation with red- and blue-detuned pulses with different intensities. For $\epsilon_B(t) \neq \epsilon_R(t)$, the Bloch-sphere precession axis $\mathbf{\Omega}(t)$ then has a finite time-dependent y component, adding more degrees of freedom to the coherent dynamics. For suitable parameter choices, such asymmetric DPE can result in Bloch-sphere trajectories that coherently evolve toward the excited state at long times.

We experimentally verify our insights by characterizing the dynamics and quality of the scattered photons under DPE of a solid-state 2LS. As discussed in detail in the following, our results confirm a maximal population transfer fidelity of approximately 50% under symmetric DPE, owing to incoherent phonon-induced dynamics. Further, we show that coherent dynamics with a population inversion of 80% are achievable through an asymmetric weighting of the red and blue components of the dichromatic pulse. We conclude our study by analyzing the quality of the resulting photons in terms of the degree of multiphoton suppression and Hong-Ou-Mandel (HOM) visibility.

As a solid-state 2LS for the dichromatic excitation experiments, we use the negatively charged exciton transition X^{1-} of a charge-tunable, planar cavity InGaAs QD sample [18,23]. Figure 2(a) shows the experimental setup to generate the dichromatic pulses for excitation. A mode-locked laser with 80.3 MHz repetition rate and 160 fs pulse width is sent to a folded $4f$ setup, which consists of lenses, beam expanders (BEs), a grating, a set of two motorized razor blades (RBs), and a beam block. The RBs control the overall spectral width of the diffracted beam, while a beam block placed between them removes the undesired frequency component resonant with the zero-phonon line, simultaneously ensuring phase locking. After backreflection on a mirror, the remaining light recombines on the same grating and gets coupled into an optical fiber before exciting the QDs. Figure 2(b) depicts an example of the spectra of the excitation laser and the absorption profile of
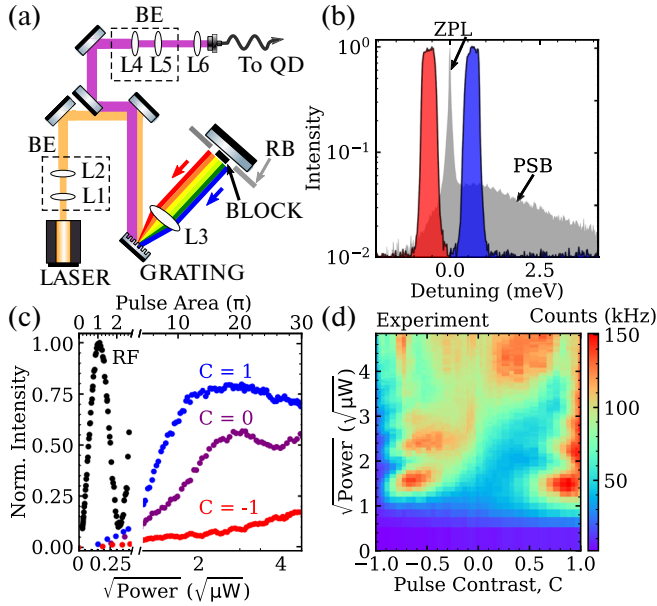
FIG. 2. Experimental setup, spectral properties, and QD emission intensity under dichromatic pulse excitation. (a) Schematic of the folded $4f$ experimental setup for pulsed excitation (L, lenses). (b) Spectra of the excitation laser (red and blue) and the QD absorption (mirrored from the emission spectra, gray), as measured on the spectrometer. Spectral filtering with a bandwidth of 120 μeV after the collection fiber isolates the ZPL from the PSB and excitation laser. (c) Emission count rate as a function of excitation power using a single resonant pulse (RF), the red sideband ($C = -1$), blue sideband ($C = 1$), and an equally weighted combination of the two ($C = 0$), normalized to the maximum intensity obtained via RF excitation. (d) Experimental data on the emission count rate as a function of pulse area and pulse contrast, defined as the weighted difference between the integrated intensity of the red and blue sidebands. Changes in the pulse contrast are implemented by varying the width of blue or red sidebands.

the QDs, detuned from the zero-phonon line (ZPL) at $\omega_0 = 1.280$ eV(968.8 nm), measured using a spectrometer with $\sim$30 μeV resolution. The spectrum of the QDs shows an atomiclike ZPL, along with a broad, asymmetric phonon sideband (PSB) arising primarily from interaction with longitudinal acoustic phonons [23,24]. The excitation laser spectrum shows the spectral width and the separation of the red and blue sideband of 0.5 and 1.2 meV, respectively. We define the pulse contrast C of the dichromatic pulse as a function of the integrated intensity of the red (I_R) and blue (I_B) sideband, as $C = (I_B - I_R)/(I_B + I_R)$. Finally, after filtering on the ZPL, the scattered photons are detected on a superconducting nanowire single-photon detector with $\sim$90% detection efficiency at $\sim$950 nm.

We first compare the experiment results for symmetric dichromatic driving ($C = 0$), blue-detuned excitation ($C = 1$), and red-detuned excitation ($C = -1$) with that obtained via pulsed resonant fluorescence (RF). These results are depicted in Fig. 2(c). While we observe the

expected Rabi oscillation under RF, we record much higher emission intensities at $C = 1$ than at $C = -1$, consistent with findings from previous studies and corresponding to phonon-assisted excitation [25,26]. Contrary to the expected minimal state occupation for an ideal 2LS under symmetric dichromatic excitation at $C = 0$ (cf. Fig. 1), we observe a population inversion fidelity of $\approx$50% at a pulse area of $\sim$20π. We attribute this to the unavoidable electron-phonon interaction: as discussed, phonon-induced thermalization allows occupations of $\lesssim$50%, compared to only vanishingly small levels for a dissipationless 2LS.

We now proceed to characterize the dynamics of the system under asymmetric DPE. To achieve this, an additional beam block mounted on a motorized translation stage is added in front of the RBs to allow independent control of the width of the red or blue sideband. The excitation pulse is split via a 99/1 fiber beam splitter, with the low power channel sent to the spectrometer to estimate the pulse contrast and the higher power channel used to excite the QDs. Figure 2(d) shows the experimental measured emission count rate as a function of pulse contrast and excitation power. We compare the experimental data with simulations using a numerically exact real-time path-integral formalism [27] with parameters typical of GaAs QDs [28] and employing a pair of rectangular driving pulses. We refer to Sec. I in the Supplemental Material [29] for full simulation parameters. The simulation, taking into account the exciton-phonon coupling in Fig. 3(a), shows close qualitative agreement with the experimental data. For comparison, the dynamics obtained in the absence of exciton-phonon coupling is depicted in Fig. 3(b). Figures 3(a) and 3(b) both feature oscillations in the excited state population at $C \approx \pm 0.65$, indicating their coherent nature. The nonoscillatory revival of the population inversion at $C = 1$, as well as a higher inversion efficiency at $C \approx 0.8$ where the blue sideband dominates (compared to $C = -0.65$), are found only in the presence of phonon coupling. This confirms the presence of phonon-assisted excitation. Figure 3(c) shows the line cuts of the experimental and simulated data from Figs. 2(d) and 3(a) taken at $C = -0.65$ and 1, respectively; this indicates good qualitative agreement between experiment and theory.

To better illustrate the coherent dynamics of the asymmetric pulses, in Fig. 3(d) we present simulated 2LS population dynamics on the Bloch sphere for a pulse area up to the first coherent oscillation in Fig. 3(c) at $C = -0.65$. In the absence of dissipation (top), the state of the 2LS remains pure and is constrained to the surface of the Bloch sphere. The nontrivial spiraling trajectory is a consequence of the time-dependent x and y components of the effective electric field associated with the asymmetric pulse. In this particular instance, the trajectory evolves toward the excited state located at the north pole. When the interaction with phonons is accounted for (bottom), the system features mixed-state dynamics that are no longer
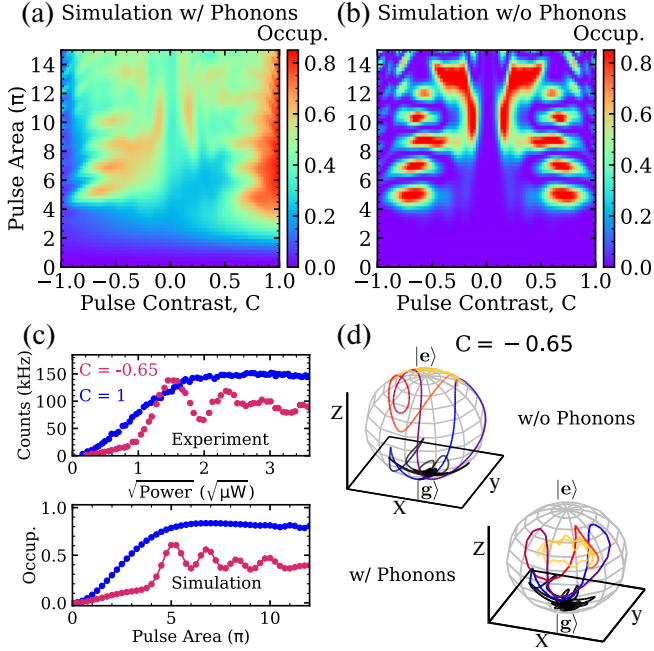
FIG. 3. Coherent dynamics of a 2LS under symmetric and asymmetric dichromatic excitation. Simulated (a) with phonons and (b) without phonons data on the emission count rate as a function of pulse area and pulse contrast, defined as the weighted difference between the integrated intensity of the red and blue sidebands. (c) Comparison between the experimental data (top) and the simulated data in the absence of phonons (bottom) at $C = -0.65$ (magenta) and $C = 1$ (blue). (d) Simulated dynamics of the first oscillation maxima (pulse area of 5π), for asymmetric dichromatic excitation ($C = -0.65$) from calculations without (top) and with (bottom) phonon coupling, indicate complete (incomplete) population inversion without (with) phonon coupling. Darker colors represent earlier times. The 2LS is initialized in the ground state $|g\rangle$.

FIG. 4. Single-photon purity and indistinguishability under asymmetric dichromatic excitation at $C = -0.65$. (a) Measurement of the second-order correlation function gives $g^{(2)}(0) = 0.016(1)$. (b) Two-photon interference of consecutively scattered photons delayed by 12.5 ns, prepared in cross ($g_\perp^{(2)}$) and parallel ($g_\parallel^{(2)}$) polarizations. Here, the 120 μeV bandwidth spectral filter is used to isolate the ZPL from the excitation laser. (c) Closeup of the zero delay peak for $g_\parallel^{(2)}$ reveals a dip, due to temporal filtering from our detectors. Dashed (green) and solid (orange) lines represent the convolved and the deconvolved fit to the experimental data (solid circles), respectively. (d) Two-photon interference visibility V_{HOM} as a function of the integration time window for $g_{\parallel(\perp)}^{(2)}$ around $\tau = 0$. The solid (dashed) line is obtained from integrating the convolved (deconvolved) fit in (c).

restricted to the surface of the Bloch sphere. Qualitatively, the spiraling trajectory still looks similar to that of the phonon-free case. However, now the excited state is no longer reached. Rather, the projection onto the z axis gives a final excited state population of $\approx 60\%$. Note that this value is lower than the measured 80% inversion fidelity, likely due to a slight mismatch in the pulse shape between simulation and experiment. In any case, our combined results indicate that for $C \approx -0.65$ phonons certainly quantitatively affect the dynamics, but dominating coherent oscillations nonetheless survive. In contrast, for positive pulse contrast, the higher maxima of the coherent oscillations are strongly suppressed by the interaction with phonons. This qualitative difference in population between positive and negative pulse contrast is attributable to the differing spectral overlap of the dichromatic pulse pair with the QD's phonon sideband (cf. Fig. 2).

Richer and even more complex dynamics emerge when moving beyond the case of a 2LS [38,39]. In Sec. VII of the Supplemental Material [29], we present spectroscopic
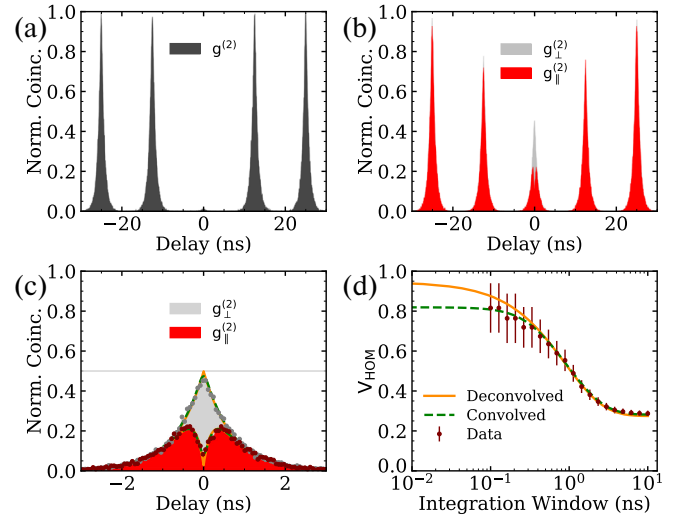
results from the neutral exciton, which has a fine-structure splitting and an excited biexciton state close in energy.

Having identified the pulse contrast and excitation power to optimize the emission count rate, we proceed to characterize the single-photon performance from our QDs under DPE. By sending the photons into a Hanbury-Brown and Twiss interferometer, we observe multiphoton suppression of $g^{(2)}(0) = 0.016(1)$, indicating high purity single-photon emission, as shown in Fig. 4(a). We then measure the indistinguishability of the scattered photons via HOM interference between two consecutively emitted photons at a time delay of 12.5 ns. The figure of merit here is the two-photon interference visibility V_{HOM}, determined by sending the photons into an unbalanced Mach-Zehnder interferometer with an interferometric delay of 12.5 ns to temporally match the arrival time of subsequently emitted photons on the beam splitter. Figures 4(b) and 4(c) show the normalized HOM histogram as a function of time delay τ between detection events for photons prepared in cross ($g_\perp^{(2)}$) and parallel ($g_\parallel^{(2)}$) polarizations within a 60 ns window and a 6 ns wide enlargement into the central peak, respectively. This closeup on the copolarized $g_\parallel^{(2)}$ peak near the zero delay illustrates the characteristic dip.

We fit the experimental data xwith the function $g_{\parallel}^{(2)}(\tau) = 0.5 \exp(-\tau/T_1)[1 - \text{V}_{\text{HOM}}^{\text{deconv}} \times \exp(-\tau/\tau_C)]$ [40–43], convolved with a Gaussian instrument response function (bandwidth of 0.168 ns), where the independently measured lifetime is $T_1 = 687(3)$ ps. This yields a deconvolved visibility of $\text{V}_{\text{HOM}}^{\text{deconv}} = 0.95(1)$ and a $1/e$ width of $\tau_C = 0.33(2)$ ns. The signature dip around the zero delay, usually present under nonresonant pumping and resonant two-photon excitation schemes, indicates deviation from the transform limit and thus imperfect photon wave packet coherence. The width of the dip corresponds to the characteristic time of $T_2^* = 2\tau_C = 0.66(4)$ ns for the inhomogeneous broadening of the emitter due to pure dephasing or timing jitter in emission [40,44]. We speculate that this may be dominated by phonon-induced dephasing, as we observe a narrower dip under phonon-assisted excitation while noting its absence under strict monochromatic resonant excitation. See Secs. III and IV in the Supplemental Material [29] for the corresponding experimental evidence and discussion. Figure 4(d) shows V_{HOM} as a function of integration window around $\tau = 0$ for temporal filtering of events between detection. Temporal postselection [41] increases the raw visibility, V_{HOM} from 0.29(2) to 0.81(12) when narrowing the integration time window from 10 to 0.1 ns, respectively. Integrating the fit function to $g_{\parallel(\perp)}^{(2)}$ (solid lines) gives a maximum convolved (deconvolved) visibility of $\text{V}_{\text{HOM}} = 0.81(0.95)$. The presence of residue coincidences around the zero delay in the histogram for scattered photons under DPE indicates the effect of finite time jitter and dephasing in the photon coherence, rendering the scheme partially coherent.

In summary, we have shown that, counterintuitively, symmetric dichromatic excitation is unsuitable for achieving coherent population control of quantum emitters. Specifically, it suffers from excitation inefficacy due to cancellation of the accumulated pulse area, and the inversion efficiency scales with the spectral overlap of the driving pulses with the emitter resonance. This nullifies the purported advantage of separating the spectrum of the driving field from the emitter zero-phonon line for background-free photon extraction. Recognizing this problem, we demonstrate that a simple adjustment in the relative weighting of the red- and blue-detuned pulses is sufficient to improve the population inversion efficiency while maintaining minimal spectral overlap. Unity population inversion is then possible for an ideal 2LS, and we have measured 80% inversion efficiency with our QD sample. The presence of intensity oscillations under asymmetric driving demonstrates the coherent nature of the observed dynamics, yet those dynamics deviate from canonical Rabi oscillations and intrinsically feature nontrivial and complex Bloch-sphere trajectories. Our Letter has further experimentally demonstrated excellent multiphoton suppression and high levels of photon indistinguishability (via temporal filtering) for such an asymmetric dichromatic excitation approach. This provides a new route to coherently excite quantum emitters, opening the prospect of background-free single-photon extraction with suitably optimized cavity-coupled photonic solid-state devices [45–47].

*To whom correspondence should be addressed.
 zk49@hw.ac.uk
†To whom correspondence should be addressed.
 b.d.gerardot@hw.ac.uk
‡Present address: Leiden University, P.O. Box 9504, 2300 RA Leiden, The Netherlands.
§Present address: Centre for Engineered Quantum Systems, School of Mathematics and Physics, University of Queensland, QLD 4072, Australia.

[1] J. L. O'Brien, A. Furusawa, and J. Vučković, Photonic quantum technologies, Nat. Photonics **3**, 687 (2009).

[2] H. de Riedmatten, I. Marcikic, W. Tittel, H. Zbinden, D. Collins, and N. Gisin, Long Distance Quantum Teleportation in a Quantum Relay Configuration, Phys. Rev. Lett. **92**, 047904 (2004).

[3] B. Hensen, H. Bernien, A. E. Dréau, A. Reiserer, N. Kalb, M. S. Blok, J. Ruitenberg, R. F. L. Vermeulen, R. N. Schouten, C. Abellán, W. Amaya, V. Pruneri, M. W. Mitchell, M. Markham, D. J. Twitchen, D. Elkouss, S. Wehner, T. H. Taminiau, and R. Hanson, Loophole-free Bell inequality violation using electron spins separated by 1.3 kilometres, Nature (London) **526**, 682 (2015).

[4] S.-K. Liao *et al.*, Satellite-to-ground quantum key distribution, Nature (London) **549**, 43 (2017).

[5] P. Senellart, G. Solomon, and A. White, High-performance semiconductor quantum-dot single-photon sources, Nat. Nanotechnol. **12**, 1026 (2017).

[6] A. V. Kuhlmann, J. H. Prechtel, J. Houel, A. Ludwig, D. Reuter, A. D. Wieck, and R. J. Warburton, Transform-limited single photons from a single quantum dot, Nat. Commun. **6**, 8204 (2015).

[7] B. Kambs and C. Becher, Limitations on the indistinguishability of photons from remote solid state sources, New J. Phys. **20**, 115003 (2018).

[8] S. Gerhardt, J. Iles-Smith, D. P. S. McCutcheon, Y.-M. He, S. Unsleber, S. Betzold, N. Gregersen, J. Mørk, S. Höfling, and C. Schneider, Intrinsic and environmental effects on the interference properties of a high-performance quantum dot single-photon source, Phys. Rev. B **97,** 195432 (2018).

[9] H. Wang *et al.*, Towards optimal single-photon sources from polarized microcavities, Nat. Photonics **13,** 770 (2019).

[10] N. Tomm, A. Javadi, N. O. Antoniadis, D. Najer, M. C. Löbl, A. R. Korsch, R. Schott, S. R. Valentin, A. D. Wieck, A. Ludwig, and R. J. Warburton, A bright and fast source of coherent single photons, arXiv:2007.12654.

[11] C. Gustin and S. Hughes, Efficient pulse-excitation techniques for single photon sources from quantum dots in optical cavities, Adv. Quantum Technol. **3,** 1900073 (2020).

[12] M. Reindl, J. H. Weber, D. Huber, C. Schimpf, S. F. C. da Silva, S. L. Portalupi, R. Trotta, P. Michler, and A. Rastelli, Highly indistinguishable single photons from incoherently excited quantum dots, Phys. Rev. B **100,** 155420 (2019).

[13] S. E. Thomas, M. Billard, N. Coste, S. C. Wein, Priya, H. Ollivier, O. Krebs, L. Tazaïrt, A. Harouri, A. Lemaitre, I. Sagnes, C. Anton, L. Lanco, N. Somaschi, J. C. Loredo, and P. Senellart, Bright polarized single-photon source based on a linear dipole, arXiv:2007.04330.

[14] J. Liu, R. Su, Y. Wei, B. Yao, S. F. C. da Silva, Y. Yu, J. Iles-Smith, K. Srinivasan, A. Rastelli, J. Li, and X. Wang, A solid-state source of strongly entangled photon pairs with high brightness and indistinguishability, Nat. Nanotechnol. **14,** 586 (2019).

[15] Y. He, Y.-M. He, Y.-J. Wei, X. Jiang, M.-C. Chen, F.-L. Xiong, Y. Zhao, C. Schneider, M. Kamp, S. Höfling, C.-Y. Lu, and J.-W. Pan, Indistinguishable Tunable Single Photons Emitted by Spin-Flip Raman Transitions in InGaAs Quantum Dots, Phys. Rev. Lett. **111,** 237403 (2013).

[16] C. Simon and J.-P. Poizat, Creating Single Time-Bin-Entangled Photon Pairs, Phys. Rev. Lett. **94,** 030502 (2005).

[17] T. Huber, A. Predojević, H. Zoubi, H. Jayakumar, G. S. Solomon, and G. Weihs, Measurement and modification of biexciton-exciton time correlations, Opt. Express **21,** 9890 (2013).

[18] R. N. E. Malein, T. S. Santana, J. M. Zajac, A. C. Dada, E. M. Gauger, P. M. Petroff, J. Y. Lim, J. D. Song, and B. D. Gerardot, Screening Nuclear Field Fluctuations in Quantum Dots for Indistinguishable Photon Generation, Phys. Rev. Lett. **116,** 257401 (2016).

[19] Z. Sun, A. Delteil, S. Faelt, and A. Imamoğlu, Measurement of spin coherence using raman scattering, Phys. Rev. B **93,** 241302(R) (2016).

[20] A. J. Ramsay, A. V. Gopal, E. M. Gauger, A. Nazir, B. W. Lovett, A. M. Fox, and M. S. Skolnick, Damping of Exciton Rabi Rotations by Acoustic Phonons in Optically Excited InGaAs/GaAs Quantum Dots, Phys. Rev. Lett. **104,** 017402 (2010).

[21] L. Monniello, C. Tonin, R. Hostein, A. Lemaitre, A. Martinez, V. Voliotis, and R. Grousson, Excitation-Induced Dephasing in a Resonantly Driven InAs/GaAs Quantum Dot, Phys. Rev. Lett. **111,** 026403 (2013).

[22] Y.-M. He, H. Wang, C. Wang, M.-C. Chen, X. Ding, J. Qin, Z.-C. Duan, S. Chen, J.-P. Li, R.-Z. Liu, C. Schneider, M. Atatüre, S. Höfling, C.-Y. Lu, and J.-W. Pan, Coherently driving a single quantum two-level system with dichromatic laser pulses, Nat. Phys. **15,** 941 (2019).

[23] Z. X. Koong, D. Scerri, M. Rambach, T. S. Santana, S. I. Park, J. D. Song, E. M. Gauger, and B. D. Gerardot, Fundamental Limits to Coherent Photon Generation with Solid-State Atomlike Transitions, Phys. Rev. Lett. **123,** 167402 (2019).

[24] A. J. Brash, J. Iles-Smith, C. L. Phillips, D. P. S. McCutcheon, J. O'Hara, E. Clarke, B. Royall, L. R. Wilson, J. Mørk, M. S. Skolnick, A. M. Fox, and A. Nazir, Light Scattering from Solid-State Quantum Emitters: Beyond the Atomic Picture, Phys. Rev. Lett. **123,** 167403 (2019).

[25] P.-L. Ardelt, L. Hanschke, K. A. Fischer, K. Müller, A. Kleinkauf, M. Koller, A. Bechtold, T. Simmet, J. Wierzbowski, H. Riedl, G. Abstreiter, and J. J. Finley, Dissipative preparation of the exciton and biexciton in self-assembled quantum dots on picosecond time scales, Phys. Rev. B **90,** 241404(R) (2014).

[26] J. H. Quilter, A. J. Brash, F. Liu, M. Glässl, A. M. Barth, V. M. Axt, A. J. Ramsay, M. S. Skolnick, and A. M. Fox, Phonon-Assisted Population Inversion of a Single InGaAs/GaAs Quantum Dot by Pulsed Laser Excitation, Phys. Rev. Lett. **114,** 137401 (2015).

[27] M. Cygorek, A. M. Barth, F. Ungar, A. Vagov, and V. M. Axt, Nonlinear cavity feeding and unconventional photon statistics in solid-state cavity qed revealed by many-level real-time path-integral calculations, Phys. Rev. B **96,** 201201(R) (2017).

[28] B. Krummheuer, V. M. Axt, T. Kuhn, I. D'Amico, and F. Rossi, Pure dephasing and phonon dynamics in GaAs- and GaN-based quantum dot structures: Interplay between material parameters and geometry, Phys. Rev. B **71,** 235329 (2005).

[29] See Supplemental Material at http://link.aps.org/supplemental/10.1103/PhysRevLett.126.047403 for details on the simulation methods and parameters, quantum dot source, performance of the QD under monochromatic resonant fluorescence and phonon-assisted excitation, and dynamics of the emission under dichromatic pulse excitation with various pulse parameters and multilevel systems, as well as a comparison of the two-photon interference visibility of the scattered photons between the monochromatic and dichromatic scheme, which includes Refs. [30–37].

[30] A. V. Kuhlmann, J. Houel, A. Ludwig, L. Greuter, D. Reuter, A. D. Wieck, M. Poggio, and R. J. Warburton, Charge noise and spin noise in a semiconductor quantum device, Nat. Phys. **9,** 570 (2013).

[31] M. O. Scully and M. S. Zubairy, *Quantum Optics* (Cambridge University Press, Cambridge, England, 1997).

[32] M. Fox, *Quantum Optics: An Introduction*, Oxford Master Series in Physics (Oxford University Press, Oxford, 2006).

[33] J. Iles-Smith, D. P. S. McCutcheon, J. Mørk, and A. Nazir, Limits to coherent scattering and photon coalescence from solid-state quantum emitters, Phys. Rev. B **95,** 201305(R) (2017).

[34] A. Morreau and E. A. Muljarov, Phonon-induced dephasing in quantum-dot–cavity QED, Phys. Rev. B **100,** 115309 (2019).

[35] E. Schöll, L. Hanschke, L. Schweickert, K. D. Zeuner, M. Reindl, S. F. C. da Silva, T. Lettner, R. Trotta, J. J. Finley,

K. Müller, A. Rastelli, V. Zwiller, and K. D. Jöns, Resonance fluorescence of GaAs quantum dots with near-unity photon indistinguishability, Nano Lett. **19,** 2404 (2019).

[36] A. J. Ramsay, T. M. Godden, S. J. Boyle, E. M. Gauger, A. Nazir, B. W. Lovett, A. M. Fox, and M. S. Skolnick, Phonon-Induced Rabi-Frequency Renormalization of Optically Driven Single InGaAs/GaAs Quantum Dots, Phys. Rev. Lett. **105,** 177402 (2010).

[37] M. Müller, S. Bounouar, K. D. Jöns, M. Glässl, and P. Michler, On-demand generation of indistinguishable polarization-entangled photon pairs, Nat. Photonics **8,** 224 (2014).

[38] D. A. Malik, A. V. Kimel, and W. J. van der Zande, Coherent control of excited state populations in rubidium using Rabi oscillations, J. Phys. B **45,** 235002 (2012).

[39] A. Gürtler and W. J. van der Zande, Transitions Driven by a Missing Frequency, Phys. Rev. Lett. **93,** 153002 (2004).

[40] T. Legero, T. Wilk, A. Kuhn, and G. Rempe, Time-resolved two-photon quantum interference, Appl. Phys. B **77,** 797 (2003).

[41] A. Nazir and S. D. Barrett, Overcoming non-Markovian dephasing in single-photon sources through postselection, Phys. Rev. A **79,** 011804(R) (2009).

[42] P. Gold, A. Thoma, S. Maier, S. Reitzenstein, C. Schneider, S. Höfling, and M. Kamp, Two-photon interference from remote quantum dots with inhomogeneously broadened linewidths, Phys. Rev. B **89,** 035313 (2014).

[43] M. E. Reimer, G. Bulgarini, A. Fognini, R. W. Heeres, B. J. Witek, M. A. M. Versteegh, A. Rubino, T. Braun, M. Kamp, S. Höfling, D. Dalacu, J. Lapointe, P. J. Poole, and V. Zwiller, Overcoming power broadening of the quantum dot emission in a pure wurtzite nanowire, Phys. Rev. B **93,** 195316 (2016).

[44] R. B. Patel, A. J. Bennett, K. Cooper, P. Atkinson, C. A. Nicoll, D. A. Ritchie, and A. J. Shields, Quantum interference of electrically generated single photons from a quantum dot, Nanotechnology **21,** 274011 (2010).

[45] J. Iles-Smith, D. P. S. McCutcheon, A. Nazir, and J. Mørk, Phonon scattering inhibits simultaneous near-unity efficiency and indistinguishability in semiconductor single-photon sources, Nat. Photonics **11,** 521 (2017).

[46] C. Gustin and S. Hughes, Pulsed excitation dynamics in quantum-dot–cavity systems: Limits to optimizing the fidelity of on-demand single-photon sources, Phys. Rev. B **98,** 045309 (2018).

[47] E. V. Denning, J. Iles-Smith, N. Gregersen, and J. Mork, Phonon effects in quantum dot single-photon sources, Opt. Mater. Express **10,** 222 (2020).